Electronic Supplementary Material (ESI) for Analyst.

Supplementary material

Dummy Molecularly Imprinted Ratiometric Fluorescent Nanosensor for the Sensitive Detection of Guanidyl-Microcystins in Environmental Water

Ping Li[a], Hao Fu[a], Zhenyu Bai[a], Xiaoyang Feng[a], Ji Qi[b], Xingliang Song[a, *], Xueping Hu[a, *] and Lingxin Chen[b, c]

[a] School of Chemistry and Chemical Engineering, Linyi University, Linyi, 276005, P.R. China

[b] CAS Key Laboratory of Coastal Environmental Processes and Ecological Remediation, Research Center for Coastal Environmental Engineering and Technology, Yantai Institute of Coastal Zone Research, Chinese Academy of Sciences, Yantai 264003, China

[c] School of Pharmacy, Binzhou Medical University, Yantai, 264003, China

*Corresponding author.

Xingliang Song, E-mail: xlssong@yeah.net; Xueping Hu, E-mail: xuephu@yeah.net;

SI.1 The binding between template and the monomer

We studied the comparison of the relative binding capacity between the template molecule metformin and the functional monomer APTES by UV spectrophotometry. The UV absorption spectrum is shown in the Fig. S3. The larger the difference between the theoretical value and the maximum absorption peak of the mixed value, the stronger the interaction between the functional monomer and the template molecule.

The molecular charge distribution of metformin is simulated by Gaussian98, as shown in Fig. S2. The equilibrium configuration of each atom in metformin molecule in vacuum medium is simulated by Gaussian98, then optimize the data in water medium to obtain the charge of each atom of metformin. It is easy to find that the N atom on the guanidine group shows strong electronegativity, so it is easy to form intermolecular hydrogen bonds with H atom on APTES.

Furthermore, zeta potential is another important parameter that influences the relative binding capacity. As shown in Table S1, when metformin is connected to the APTES, the zeta potential of the mixture changed from positive to negative, an indication that metformin and APTES were successfully combined. Other zeta potential changes are shown in Table S1.

SI.2 Optimized conditions

SI.2.1 Influence of solvent type

Fig. S8A shows the effect of solvent on the binding properties and fluorescent behavior of CDs-FITC-SiO_2@MIP sensor to MCs. The fluorescent intensities ratio of NaCl containing salt solution to MCs is high because the salt effect has an impact on the stability of fluorescent substances, the presence of salt in the solution will affect the sonochemistry,[1] and the salt effect in intramolecular charge transfer reaction will change the kinetics of reaction rate,[2] so NaCl salt solution is selected as solvent.

SI.2.2 Influence of salt effect

Next, the influence of salt solutions with different concentrations of NaCl on the fluorescent intensities ratio of MCs was explored (Fig. S8B). The figure shows that the salt solution containing 0.5% NaCl values the highest fluorescent intensities ratio value compared with other NaCl containing solutions. Herein, the salt solution containing 0.5% NaCl was chosen for all tests to obtain the highest fluorescent intensities ratio change value.

SI.2.3 Optimization of CDs and fluorescent labeled silica spheres proportion

The ratiometric fluorescent response of CDs-FITC-SiO_2@MIP sensor depends on the fluorescent intensity at 450 nm and 620 nm, which is related to the proportion of CDs and FITC-SiO_2, respectively. To investigate the fluorescent intensity response to different volume ratios with two fluorescent materials, an optimization experiment was carried out with four different ratios (Fig. S8C). The results showed that the fluorescent intensities ratio was the highest when the volume ratio of the two fluorescent materials was 6:1. Thus, the combination of CDs and FITC-SiO_2 with a volume ratio of 6:1 was selected to build the CDs-FITC-SiO_2@MIP sensor for microcystins detection.

SI.2.4 Dosage optimization of CDs-FITC-SiO_2@MIP

The effect of the amount of CDs-FITC-SiO_2@MIP nanoparticles was also studied by changing their volume from 100 to 600 μg/mL. The results indicated that the amount of CDs-FITC-SiO_2@MIP in the solution greatly affects the detection sensitivity for microcystins assay. As the concentration of CDs-FITC-SiO_2@MIP nanoparticles increased, the fluorescent intensities ratio value of CDs-FITC-SiO_2@MIP sensor to microcystins increased, and the $I_{620/450}$ was the highest when it reached 400 μg/mL (Fig. S8D). Therefore, the amount of CDs-FITC-SiO_2@MIP was fixed at 400 μg/mL throughout this study.

SI.2.5 Influence of adsorption time

Next, the adsorption time was also optimized. As can be seen from Fig. S8E, after adding microcystin, the $I_{620/450}$ reached equilibrium after 1 min The results can be summarized as follows: at first, due to the large number of imprinted holes, the rebinding and recognition of microcystins were easy to complete; With the passage of time, a large number of sites were occupied, and it was difficult for microcystins to find suitable imprinting sites. As a result, 1 min was taken as the optimal adsorption time.

SI.2.6 Influence of adsorption temperature

Next, the adsorption temperature was optimized. As can be seen from Fig. S8F, the $I_{620/450}$ is the highest at 25 ℃, so 25 ℃ is selected as the best adsorption temperature.

SI.3 Table

Table S1. The zeta potential of APTES, metformin and the mixture.

	Zeta Potential (mV)
APTES	0.0852
Metformin	-13.5
APTES + Metformin	-0.30

Table S2. Selectivity Parameters[a] for CDs-FITC-SiO_2@MIP and Imprinting Factor.

Molecule	MIP			NIP			*IF*	*k*'
	$(F_{620}/F_{450})^*_{MIP}$	$I_{620/450\ MIP}$	k_{MIP}	$(F_{620}/F_{450})^*_{NIP}$	$I_{620/450\ NIP}$	k_{NIP}		
MC-RR	2.96	4.63	11.13	0.63	1.36	2.09	3.41	5.34
MC-LR	2.33	3.63	8.74	0.60	1.28	1.97	2.83	4.43
MC-YR	2.28	3.56	8.56	0.58	1.25	1.91	2.86	4.48
MC-LY	1.68	2.63	6.31	0.56	1.20	1.85	2.18	3.42
Domoic acid	0.27	0.42	1.00	0.30	0.65	1.00	0.64	1.00
Aflatoxin	0.37	0.57	1.37	0.33	0.70	1.08	0.81	1.27

[a]Normalized values of fluorescence intensity ratio. Normalized values are the difference in the fluorescence ratio of fluorescent NPs before and after fluorescence reaction. The fluorescence intensity ratio of MIP before fluorescence reaction,0.640; the fluorescence intensity ratio of NIP before fluorescence reaction,0.464.

Table S3. Spiked Recoveries and RSD (%) for the determination of MCs in real water samples by the developed CDs-FITC-SiO_2@MIP (n=3).

Sample	Added (μg/L)	Found (μg/L)	Recovery	RSD(%)
Binhai Lake	1	0.93	93.15	3.12
	5	5.24	104.81	3.93
	20	20.54	102.72	4.25
Tap water	1	1.09	109.12	4.12
	5	4.84	96.81	2.83
	20	19.51	97.55	3.26

Table S4. Comparison of analytical methods or products for the determination of microcystins in water samples.

Method/Product	Linear range (μg/L)	LOD (μg/L)	Detection object		Ref.
			MC-RR	MC-LR	
IOFB[a]	0.53–11.28	0.22		√	3
N/P CDs[b]	0.05−3	0.0171		√	4
DCHQ-Ph[c]	0.10−9.95	0.05		√	5
MWCNTs[d]	0–2	0.19		√	6
Dual Modal aptasensor[e]	0.1−50	0.5		√	7
MoS_2 Quantum Dots[f]	0.03−26.31	0.006		√	8
nBC/paper/anti-MCLR/MCLR[g]	0.1–100	0.017		√	9
Cu/Co nanorods[h]	0.065–45.83	0.022	√		10
DNA aptamer	0.2–2.5	0.08	√		11
LC–MS[i]	20–5000	6	√		12
paper spray ionization	0−9.1/0−5.8	1	√	√	13
MBio[j]	0.1–100	0.4	√	√	14
electrochemical sensing method	0.06-1000	0.015		√	15
OS-ELISA[k]	0.14-10000	0.14		√	16
LFA[l]	1-50	0.84		√	17
CDs-FITC-SiO_2@MIP	0.5–500	0.0132/ 0.0223	√	√	This work

[a] integrated optical fluorescence biosensor [b] nitrogen/phosphorus-codoped carbon dots
[c] phenyl-substituted diaza-18-crown-6 hydroxyquinoline [d] multiwalled carbon nanotubes [e] a dual-modal aptamer-based biosensor [f] MoS_2 Quantum Dots [g] nanobiochar particles and anti-MC-LR monoclonal antibodies on the fifilter paper [h] Cu/Co nanorods-catalyzed chemiluminescence aptasensor [i] liquid chromatography–mass spectrometry [j] portable biosensor system [k] Open sandwich Enzyme-linked Immunosorbent Assay [l] lateral flow assay.

SI.4 Figure

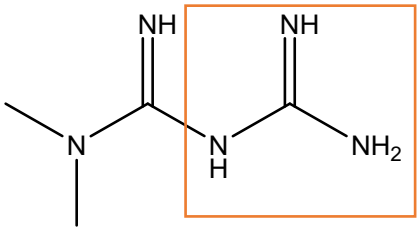

Metformin

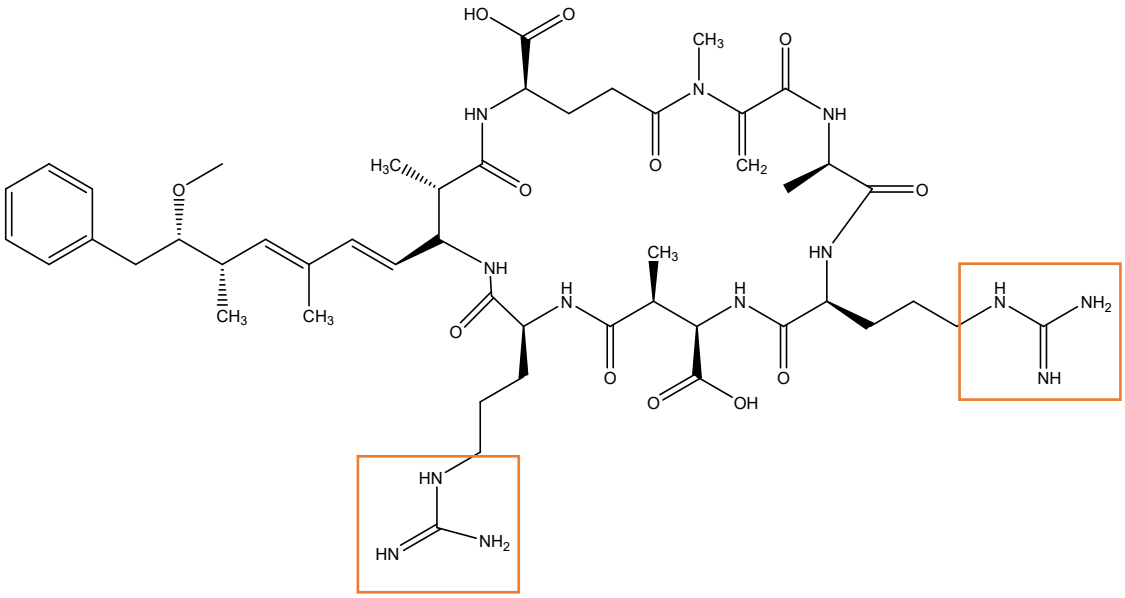

MC-RR

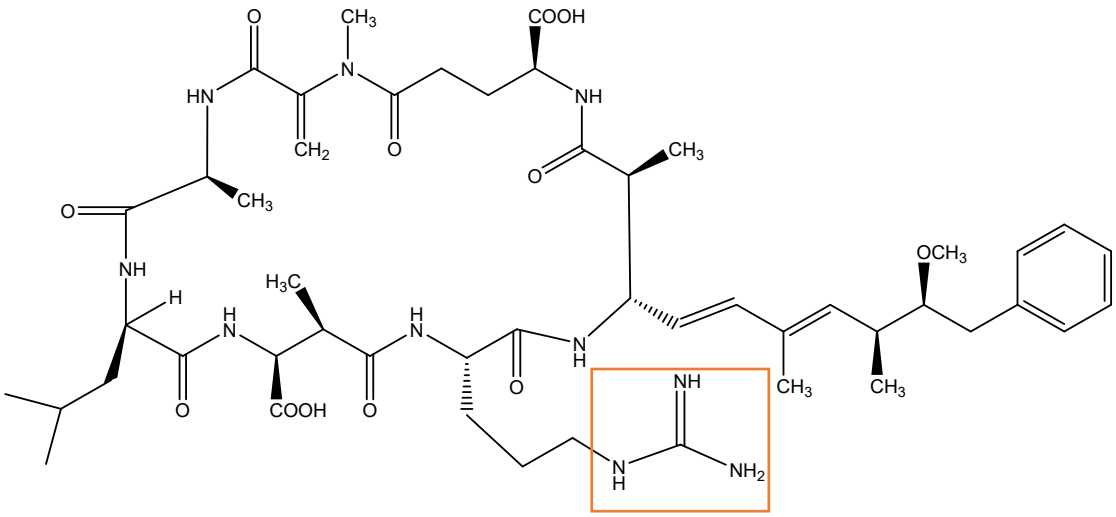

MC-LR

Fig. S1

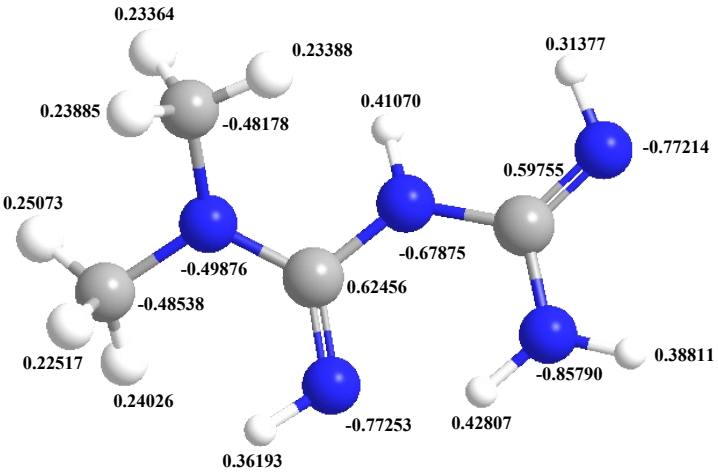

Fig. S2

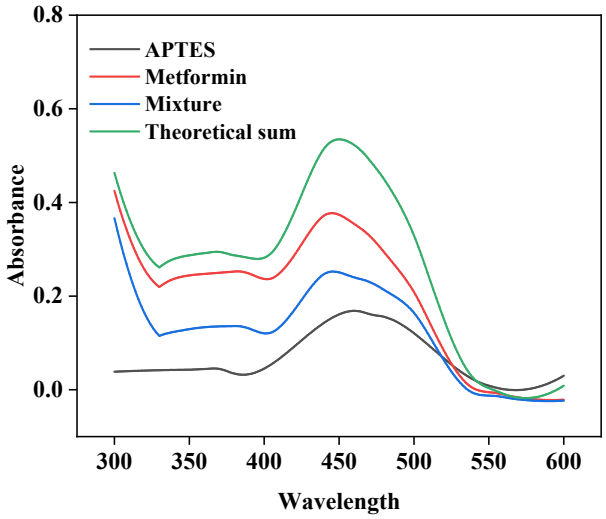

Fig. S3

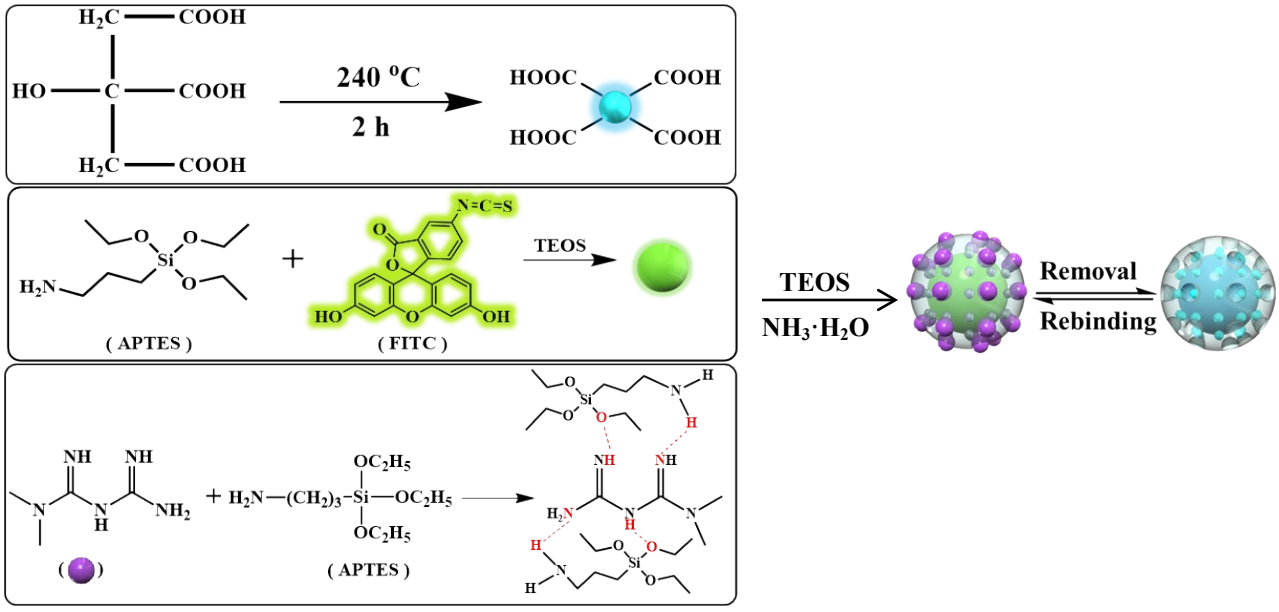

Fig. S4

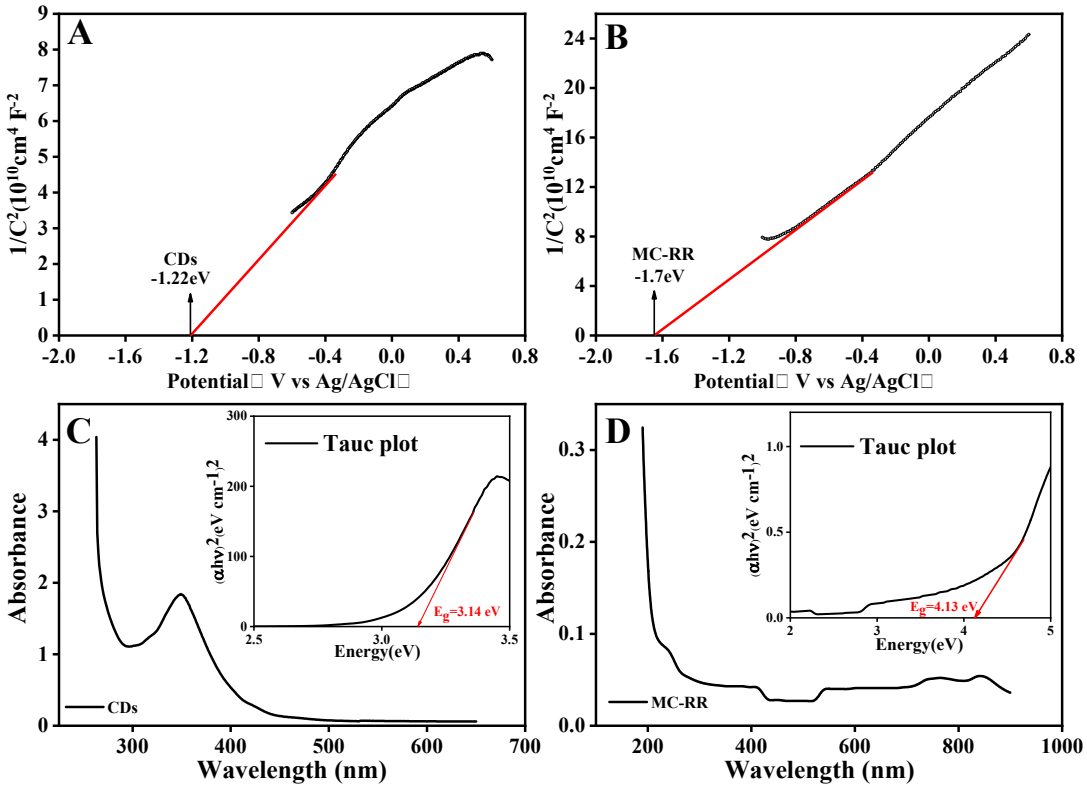
A
CDs
-1.22eV
1/C²(10¹⁰cm⁴ F⁻²
Potential□ V vs Ag/AgCl□
B
MC-RR
-1.7eV
C
Tauc plot
Eg=3.14 eV
(αhν)²(eV cm⁻¹)²
Energy(eV)
Absorbance
CDs
Wavelength (nm)
D
Tauc plot
Eg=4.13 eV
MC-RR

Fig. S5

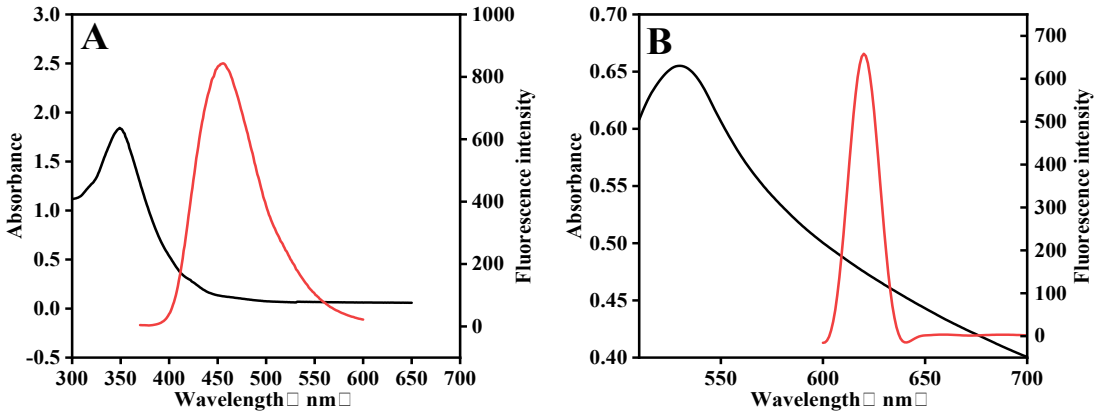
A
Absorbance
Fluorescence intensity
Wavelength□ nm□
B

Fig. S6

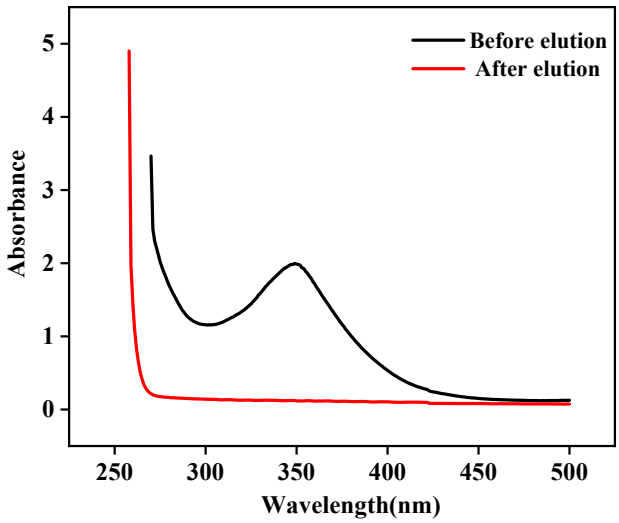
Before elution
After elution
Absorbance
Wavelength(nm)

Fig. S7

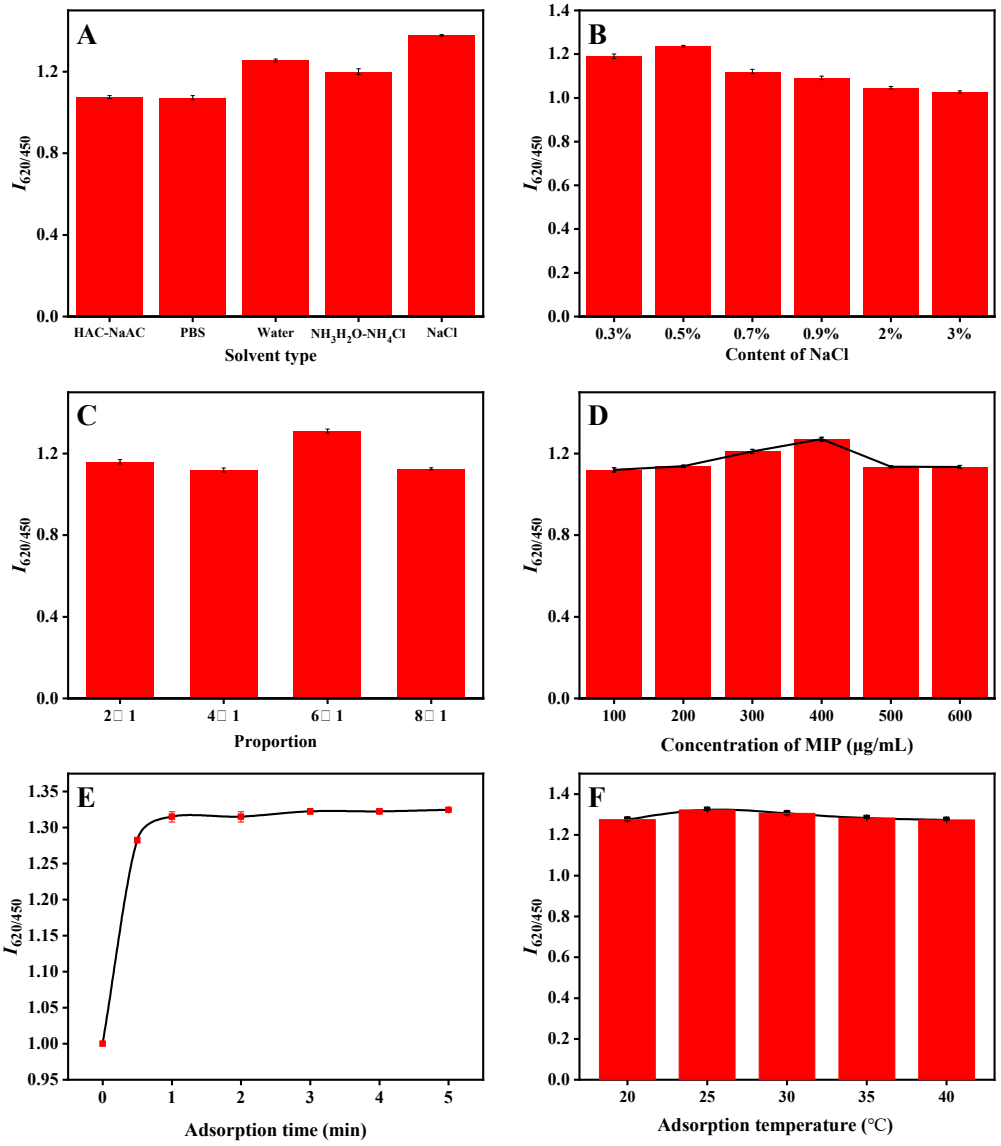

Fig. S8

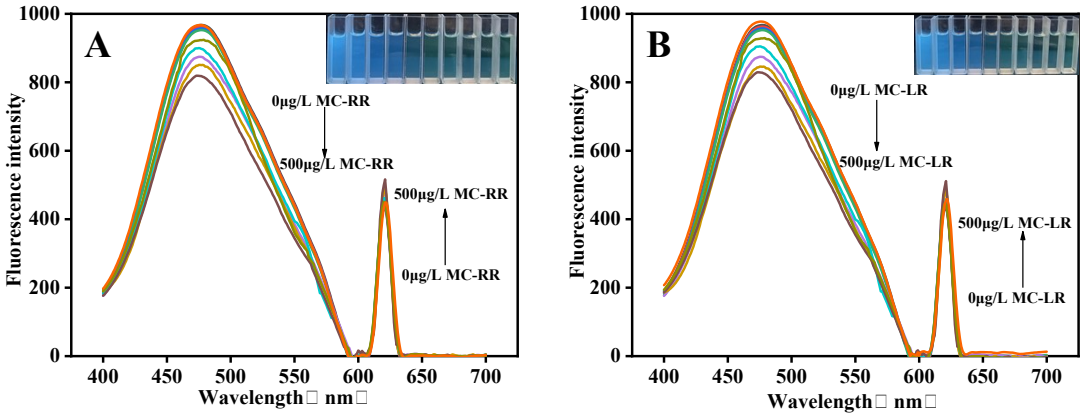

Fig. S9

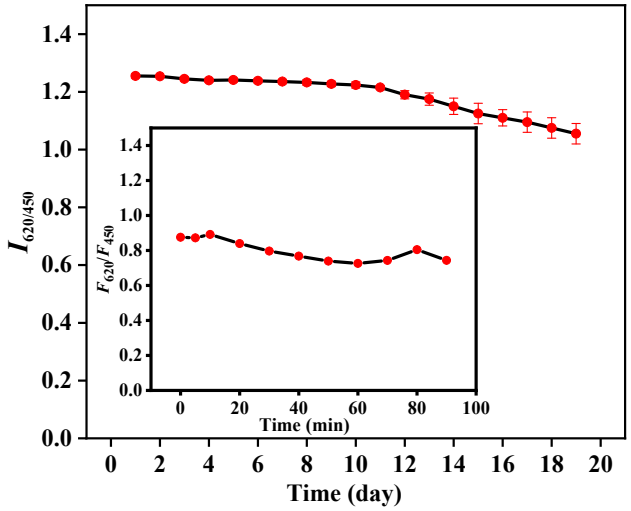

Fig. S10

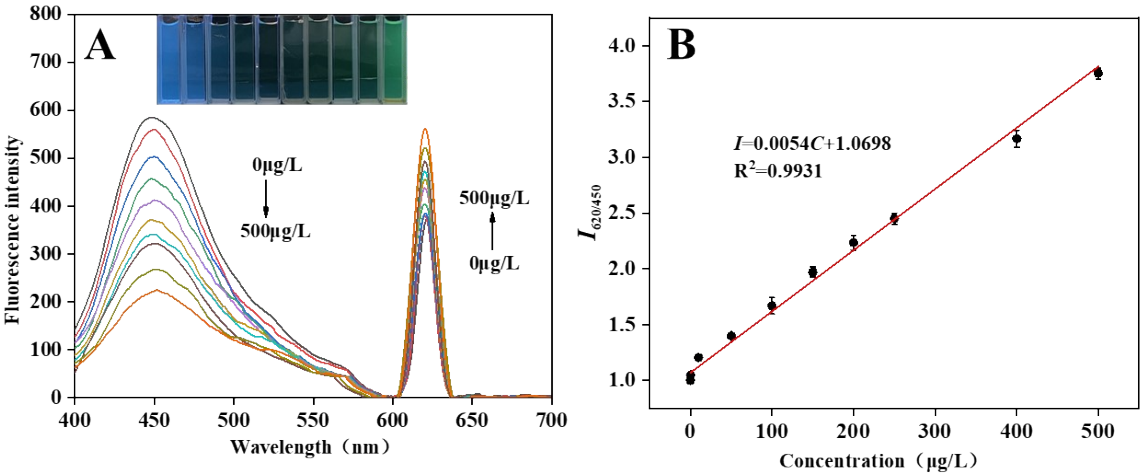

Fig. S11

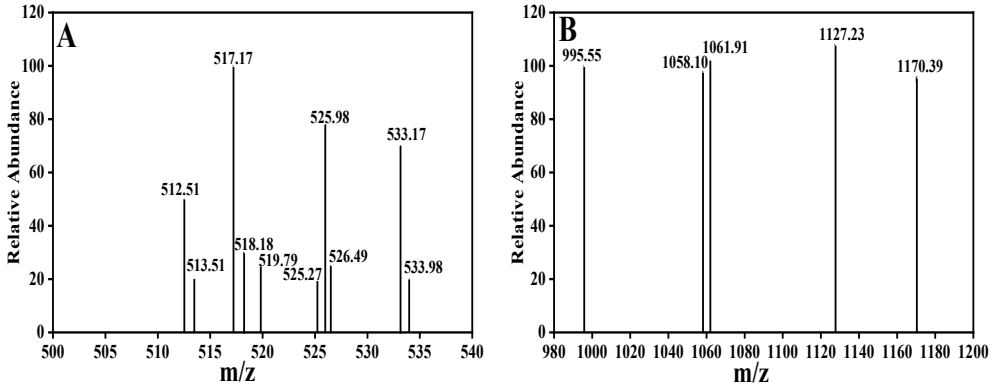

Fig. S12

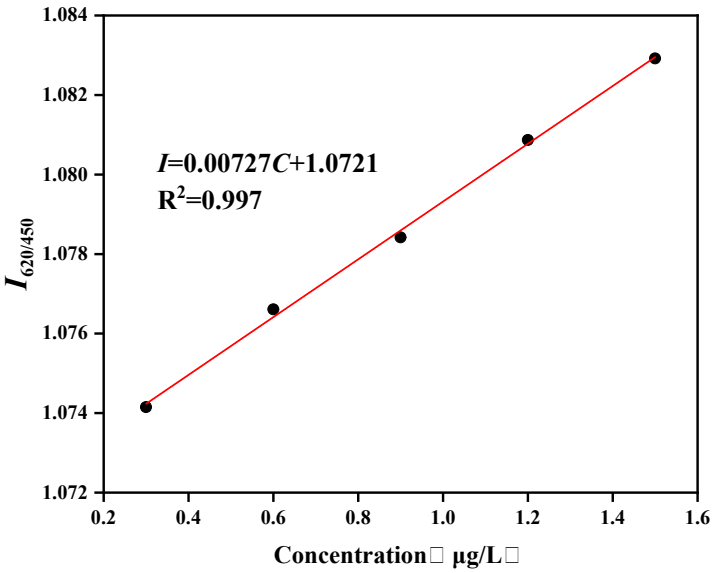

Fig. S13

SI.5 Reference

1. R. Pflieger, SI. Nikitenko and M. Ashokkumar, *Ultrason. Sonochem*, 2019, **59**, 104753.
2. Y. Kasai, N. Yoshida and H. Nakano, *J. Mol. Liq*, 2014, **200**, 32-7.
3. L. Liu, D. Shan, X. Zhou, H. Shi, B. Song and F. Falke, *Biosens. Bioelectron*, 2018, **106**, 117-21.
4. X. Wang, J. Yu, W. Ji, M. Arabi, L. Fu and B. Li, *ACS Appl. Nano Mater*, 2021, **4(7)**, 6852-60.
5. L. Lvova, C. Guanais Gonçalves, L. Prodi, M. Lombardo, N. Zaccheroni and E. Viaggiu, *Chem. Communc*, 2018, **54(22)**, 2747-50.
6. M. Lee, H. J. Kim and D. Kim, *Biosens. Bioelectron*, 2021, **192,** 113529.
7. M. Li, H. Lin, S. K. Paidi, N. Mesyngier, S. Preheim and I. Barman, *ACS Sens*, 2020, **5(5)**, 1419-26.
8. H. Cao, W. Dong, T. Wang, W. Shi, C. Fu and Y. Wu, *ACS Sustain. Chem. Eng.* 2020, **8**, 10939−10946.
9. L. Yao, L. He, Y. Yang, Y. Zhang, Z. Liu and L. Liang, *Sci. Total Environ*, 2021, **750,** 141692.
10. B. Liu, X. Li, S. Liu and X. Hun, *Microchem. J*. 2019, **145,** 648-54.
11. S. Wu, Q. Li, N. Duan, H. Ma and Z. Wang, *Microchim. Acta*, 2016, **183(9)**, 2555-62.
12. W. Li, P. Xie, J. Chen, J. He, X. Guo and D. Yu, *J. Chromatogr B*, 2014, **963,** 113-8.
13. X. Zhu, Z. Huang, W. Gao, X. Li, L. Li and H. Zhu, *J. Agric. Food Chem*, 2016, **64(27),** 5614-9.
14. S. R. Bickman, K. Campbell, C. Elliott, C. Murphy, R. O'Kennedy, P. Papst, *Environ. Sci. Technol*, 2018, **52(20)**, 11691-8.
15. K. Abnous, N. M. Danesh, M. A. Nameghi, M. Ramezani, M. Alibolandi, P. Lavaee and S. M. Taghdisi, *Biosens. Bioelectron*, 2019, **144**, 111674.
16. L. Chen, R. Tan, Y. Zhou, L. Zhang and J. Dong, *Microchem. J*, 2020, **158**, 105325.
17. J. Feng, Y. Wu, J. Zhang, R. Jin, Y. Li and Q. Shen, *J Food Compos Anal*, 2023, **115**, 105012.